

# Effective utilization of quantum-cascade distributed-feedback lasers in absorption spectroscopy

Anatoliy A. Kosterev, Robert F. Curl, Frank K. Tittel, Claire Gmachl, Federico Capasso, Deborah L. Sivco, James N. Baillargeon, Albert L. Hutchinson, and Alfred Y. Cho

A variable duty cycle quasi-cw frequency scanning technique was applied to reduce thermal effects resulting from the high heat dissipation of type I quantum-cascade lasers. This technique was combined with a 100-m path-length multipass cell and a zero-air background-subtraction technique to enhance detection sensitivity to a parts-in- $10^9$  (ppb) concentration level for spectroscopic trace-gas detection of  $\text{CH}_4$ ,  $\text{N}_2\text{O}$ ,  $\text{H}_2\text{O}$ , and  $\text{C}_2\text{H}_5\text{OH}$  in ambient air at 7.9  $\mu\text{m}$ . A new technique for analysis of dense high-resolution absorption spectra was applied to detection of ethanol in ambient air, yielding a 125-ppb detection limit. © 2000 Optical Society of America

OCIS codes: 140.5960, 280.3420, 300.6320, 010.1280.

## 1. Introduction

Recently developed quantum-cascade lasers<sup>1</sup> have been demonstrated to be useful tunable single-frequency light sources for laser-based absorption spectroscopy.<sup>2–5</sup> Compared with lead-salt diode lasers that emit in the same mid-IR region, quantum-cascade (QC) distributed-feedback (DFB) lasers deliver much higher power, provide mode-hop-free frequency tuning, and are considerably more robust. These devices are also capable of lasing at near-room temperature. A pressing issue is the development of effective methods for utilizing these lasers in absorption spectroscopy, especially for the purpose of monitoring atmospheric trace-gas species. In this paper we bring together a scheme for convenient operation of the laser in a quasi-cw mode with some of the standard tools for high-sensitivity gas monitoring to demonstrate the first steps in the creation of a portable field instrument.

The first choice to be made is whether to operate the lasers in a pulsed mode near room temperature or cw near liquid-nitrogen temperature. Clearly room-

temperature operation is convenient because it dispenses with the need for cryogenic liquids and an optical Dewar. However, strong power dissipation in the active region limits the operation of QC lasers in such conditions to pulses of several nanoseconds duration. The rapid changes of current that occur with short (nanoseconds) pulse excitation lead to frequency chirping and to an increase in laser linewidth from less than 10 MHz for cw operation to >400 MHz. Room-temperature pulsed operation also results in a greatly reduced duty cycle. Thus cw operation of a QC DFB laser at cryogenic temperatures is still advantageous for many applications, especially if a compact liquid-nitrogen Dewar is employed. A quasi-cw operation mode was adopted here.

Type I QC lasers (the only kind of QC laser capable of single-frequency mid-IR operation) dissipate as much as 10 W of power in cw operation. The high power dissipation is more than compensated for by a high conversion efficiency that produces as much as 450 mW. However, the power consumption causes a fast boil-off of liquid nitrogen and a frequency drift, which restricts data acquisition times. This is not a serious problem; it can be solved by several approaches. We have found that a convenient way to avoid these effects is to operate the laser in a quasi-cw mode, supplying current in pulses of 120–235- $\mu\text{s}$  duration at an 800–1000-Hz repetition rate. This somewhat reduces the duty cycle but does not adversely affect the frequency resolution. From each pulse a frequency scan of as much as  $2\text{ cm}^{-1}$  is produced, and a number of such scans are averaged.

To demonstrate the effectiveness of this scanning

---

A. A. Kosterev (akoster@rice.edu), R. F. Curl, and F. K. Tittel are with the Rice Quantum Institute, Rice University, Houston, Texas 77251-1892. C. Gmachl, F. Capasso, D. L. Sivco, J. N. Baillargeon, A. L. Hutchinson, and A. Y. Cho are with Bell Laboratories, Lucent Technologies, 600 Mountain Avenue, Murray Hill, New Jersey 07974.

Received 17 November 1999; revised manuscript received 13 April 2000.

0003-6935/00/244425-06\$15.00/0

© 2000 Optical Society of America

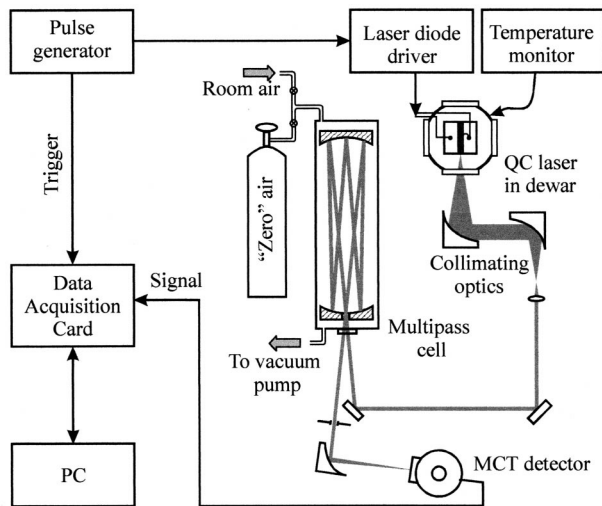


Fig. 1. Schematic of the QC DFB-based gas sensor.

method for high-sensitivity absorption spectroscopy we combined the method with the standard spectroscopic techniques of a long multipass cell (100 m) and zero-air background subtraction to obtain sub-parts-in- $10^6$  (ppm) detection sensitivities for several gases. As a demonstration,  $\text{CH}_4$ ,  $\text{N}_2\text{O}$ , and some isotopic species of  $\text{H}_2\text{O}$  in ambient air were detected near  $7.9 \mu\text{m}$  by use of a direct absorption technique and the methods described above. We also described a pattern-fitting technique for analysis of dense absorption spectra data and apply it to ultrasensitive detection of ethanol.

## 2. Experiment

A schematic of the QC DFB laser-based gas sensor configuration is shown in Fig. 1. In these experiments a QC DFB laser designed for cw operation at cryogenic temperatures near  $7.9 \mu\text{m}$  was used. The laser was placed in a liquid-nitrogen Dewar equipped with a broadband antireflection-coated ZnSe window. No active temperature stabilization was applied. Two off-axis aluminum gold-coated parabolic mirrors and an uncoated  $\text{BaF}_2$  lens were used to shape the laser beam. These optics did not collect all the QC DFB laser radiation because of the high beam divergence of the QC laser ( $\sim 65^\circ$  and  $\sim 45^\circ$  full width at half-maximum in the direction normal to and in the plane of the laser stripe, respectively) and the location of the laser far from the Dewar window. The IR power of the collimated beam was  $\sim 10 \text{ mW}$  for a laser drive current of 1 A. This power was sufficient to avoid limitation of sensitivity by detector noise. A commercial multipass cell with an effective optical path length of 100 m was used. The ambient air that we analyzed flowed continuously through the cell at 20–40 Torr to minimize pressure-broadening effects on the monitored absorption lines. After it passed through the cell, the laser radiation was focused onto a liquid-nitrogen-cooled photovoltaic HgCdTe detector with a built-in preamplifier (dc to 20-MHz bandwidth). The electrical signal was dig-

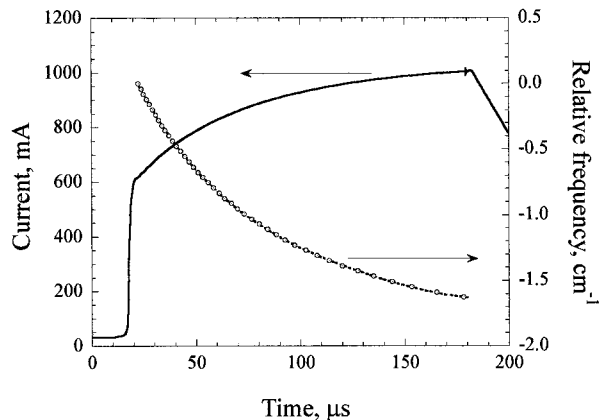


Fig. 2. Laser current and frequency as a function of time when a  $200\text{-}\mu\text{s}$ -long pulse is applied to the external modulation input of the laser current driver. Circles indicate positions of the etalon fringes. The fitting curve is a fourth-order polynomial.

itized with a 12-bit data acquisition card capable of a 50-MHz sampling rate.

If the laser is continuously driven at its practically useful current level of 600–1000 mA, the power dissipation reaches 10 W and, as mentioned above, causes fast boil-off of liquid nitrogen and frequency drift. To avoid this effect we supplied laser current in pulses of 120–235- $\mu\text{s}$  duration at an 800–1000-Hz repetition rate by applying rectangular pulses to the external modulation input of a low-noise driver (Wavelength Electronics MPL-5000). This device has a specified 7-kHz bandwidth limitation. When a rectangular pulse is applied to the external modulation input, the laser current experiences a 40- $\mu\text{s}$  delayed jump from zero to some intermediate value and then grows exponentially to a steady-state level, which permits fast scanning of the QC DFB laser frequency by use of a pulse generator. The use of a pulse generator instead of a function generator permitted easy variation of the laser duty cycle and thus of its average operating temperature and laser frequency. This scheme results in an essentially nonlinear frequency-time dependence, but the relationship between frequency and time is perfectly reproducible and the nonlinearity is easily removed during data processing. This dependence is depicted in Fig. 2, as measured with the etalon fringes from two uncoated ZnSe surfaces inserted in the laser beam. Analysis of the current-frequency dependence indicates that the frequency follows the current almost linearly, although there is small quadratic term, regardless of the rate of current change, which implies that there is no thermal inertia of the QC DFB laser on this time scale. Each current pulse resulted in a frequency scan that covered  $\sim 2 \text{ cm}^{-1}$ .

The main factors that limited sensitivity for detecting weak absorption lines were optical interference fringes and baseline inhomogeneities caused by optical diffraction and absorption of atmospheric water from air paths outside the cell. Higher-frequency fringes were created by the multipass cell but were

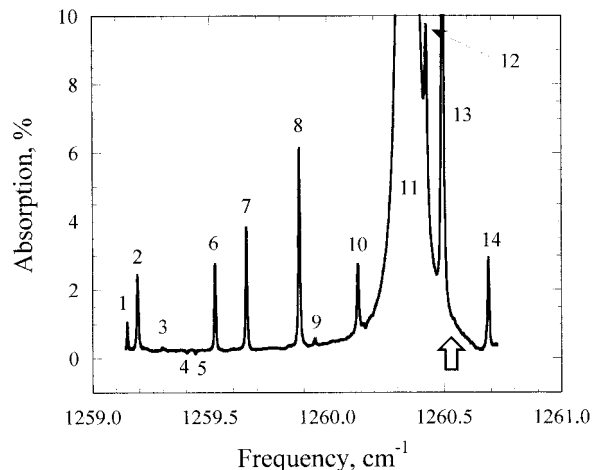


Fig. 3. Example of an absorption spectrum of room air obtained with a 100-m path-length multipass cell and a zero-air background-subtraction technique. The assignment of the strong spectral lines is 1, 11, 13,  $\text{H}_2^{16}\text{O}$ ; 2, 3, 10,  $\text{N}_2\text{O}$ ; 6–8, 14,  $\text{CH}_4$ ; 9,  $\text{H}_2^{18}\text{O}$ ; 12,  $\text{HDO}$ ; 4, 5,  $\text{CO}_2$  in the reference zero-air that appears as a negative absorption. An arrow marks a position of the  $^{13}\text{CH}_4$  absorption line shown in Fig. 4.

almost completely washed out by application of a weak changing mechanical force to the multipass cell during the measurements. To suppress the influence of other interfering effects we used a zero-air background-subtraction technique.<sup>6</sup> Spectra of ambient air and pollutant-free synthetic air (zero air) were taken alternately. Replacing the air in the 3.3-L multipass cell required  $\sim 30$  s. The zero-air signal (as a function of a data-point number) was subtracted from the ambient air signal, and the result was normalized to the zero-air signal, yielding an absorption spectrum. In most of the measurements, pure air with the addition of 5%  $\text{CO}_2$  was used as a zero gas. The resultant weak negative-absorption  $\text{CO}_2$  lines in the acquired spectra aided in the spectral calibration of wavelength scans.

### 3. Detection of $\text{CH}_4$ , $\text{N}_2\text{O}$ , and $\text{H}_2\text{O}$ in Ambient Air

A typical absorption spectrum of ambient air obtained with a QC DFB laser by the procedure described in Section 2 is shown in Fig. 3. Four strong  $\text{CH}_4$  lines, two strong  $\text{N}_2\text{O}$  lines, and several  $\text{H}_2\text{O}$  lines corresponding to different isotopic species fall into the spectral range covered by this frequency scan. The spectrum depicted is the result of averaging 6000 individual scans for both ambient air and zero air. The acquisition and averaging of 6000 200- $\mu\text{s}$ -long scans with 50 megasamples/s at a 1-kHz repetition rate required approximately 30 s. Optimized software should permit faster data acquisition by utilizing a larger fraction of the current pulses.

We determined the  $\text{CH}_4$  and  $\text{N}_2\text{O}$  concentration levels in ambient air by fitting the envelopes of the stronger absorption lines with a Voigt function. The area under a fitting curve was compared with that predicted from the HITRAN database. The accuracy of these measurements is limited by the slow

Table 1. Measured Concentrations of Several Ambient Air Components

Air Component	Line Center ( $\text{cm}^{-1}$ )	Measured Peak Absorbance ( $\times 10^{-2}$ )	Calculated Concentration (ppm)
$\text{CH}_4$	1259.884	2.74	1.914
$\text{CH}_4$	1259.661	1.68	1.970
$\text{CH}_4$	1259.525	1.19	1.913
$\text{N}_2\text{O}$	1259.194	1.02	0.272
$\text{H}_2\text{O}$	1259.148	0.39	$1.74 \times 10^4$ (55% relative humidity)

variations of the baseline, which may contribute to the pressure-broadened spectral line wings. To obtain some estimate of this measurement error we calculated the  $\text{CH}_4$  concentration, using three different absorption lines from the same frequency scan. The  $\text{CH}_4$  results are listed in Table 1 together with the  $\text{N}_2\text{O}$  concentration as measured with a line at  $1259.194 \text{ cm}^{-1}$ . [The absorbance in Table 1 is  $-\log_{10}(T)$ , where  $T$  is the transmission.] The measurement accuracy is estimated to be 1.5%, based on the  $\text{CH}_4$  concentrations obtained from the intensities of three different absorption lines.

The sensitivity to weak absorption features is limited by an unstable baseline. This limitation can be minimized if a reproducible multipass cell deformation is applied. To estimate the minimum detectable absorbance we used the same technique as reported in our earlier paper.<sup>2</sup> It consisted of selecting a part of the spectrum that contained no absorption lines and setting the fitting procedure parameters to find an absorption feature similar to a  $\text{CH}_4$  absorption line. The typical peak absorbance of such a feature did not exceed  $\pm 3.5 \times 10^{-5}$ , or  $8 \times 10^{-5}$  fractional absorption. For the strongest absorption lines in these experiments, a detection limit of 2.5 parts in  $10^9$  (ppb) for  $\text{CH}_4$ , 1.0 ppb for  $\text{N}_2\text{O}$ , and 60 ppb for  $\text{H}_2\text{O}$  (absorption line at  $1260.344 \text{ cm}^{-1}$ ) is estimated.

Measurement of isotopic composition is of interest as a means for determining the sources and sinks of trace-gas constituents.<sup>7</sup> Absorption lines of  $\text{H}^{18}\text{O}$  and  $\text{HD}^{16}\text{O}$  were clearly observed in the spectra, as illustrated in Fig. 3. It was possible to detect a  $^{13}\text{CH}_4$  line on the shoulder of the  $\text{H}_2\text{O}$  line (Fig. 4), which in principle permits the measurement of the isotopic composition of water vapor and  $\text{CH}_4$  in ambient air from the intensities of the isotopic absorption lines. The accuracy of such measurements must be at least  $\sim 10\%$  (where  $\%$  is parts in  $10^3$ ) in terms of relative deviations from an isotopic standard to be of practical interest. The present precision of line intensity measurements in our experiments is  $\sim 1.5\%$  for spectral lines with several-percent peak absorption. This degree of precision leads to a standard deviation of  $\sim 2\%$ , or  $20\%$  for the intensity ratio calculations, which is not good enough. However,

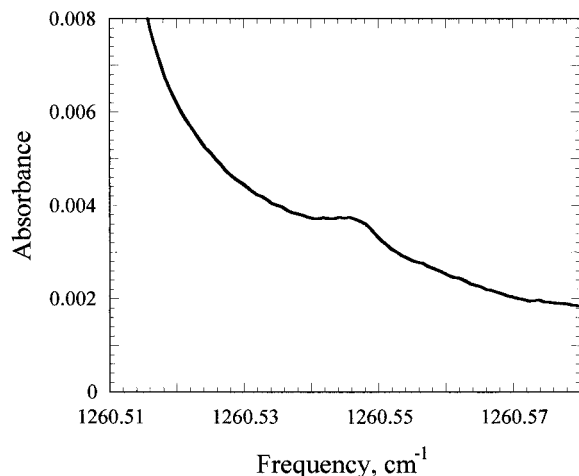


Fig. 4. Detected  $^{13}\text{CH}_4$  absorption line at  $1260.547\text{ cm}^{-1}$  on the shoulder of a  $\text{H}_2\text{O}$  line.

we believe that the accuracy of intensity measurements will be improved in the future.

We calculated the abundance of HDO in ambient air by comparing the intensity of the HDO  $\nu_2 P(5)$  line at  $1260.423\text{ cm}^{-1}$  with the intensity of the  $\text{H}_2^{16}\text{O}$   $\nu_2 P(12)$  line at  $1260.498\text{ cm}^{-1}$ . A line intensity  $A$  was defined as an area under the best-fitting Voigt curve. The ratio of intensities  $R = A(\text{HDO})/A(\text{H}_2\text{O})$  was then compared with the data available from the HITRAN database, in which the abundance is assumed to be  $\delta D = 0$  as referred to the Vienna Standard Mean Ocean Water (V-SMOW) isotopic standard.<sup>8</sup> The V-SMOW concentration ratio was  $[\text{HDO}]/[\text{H}_2\text{O}] = 3.115 \times 10^{-4}$ . Three independent measurements yielded values of  $\delta D = -100\text{‰}$ ,  $\delta D = -160\text{‰}$ , and  $\delta D = -50\text{‰}$ , for an average value of  $\delta D = -103\text{‰}$  with an estimated standard deviation of  $45\text{‰}$ . This value is reasonable, because according to the Global Network for Isotopes in Precipitation (GNIP) data base  $\delta D$  varies from 0 to  $-300\text{‰}$  with geographic region and time and can experience a  $100\text{‰}$  change in one month.<sup>9</sup> The scatter of our results is probably caused by a strong temperature dependence of the  $\text{H}_2^{16}\text{O}$   $\nu_2 P(12)$  line intensity, which has a lower-state energy of  $2275\text{ cm}^{-1}$ . The temperature sensitivity of the intensity ratio of the two lines being compared is  $dR/dT = -3\text{‰}/^\circ\text{C}$ . The isotopic composition measurements reported above were separated by several hours. Improved temperature control and more-accurate intensity measurements should result in more-reliable isotopic measurements.

#### 4. Detection of Ethanol

The spectral range near  $8\text{ }\mu\text{m}$  is also useful for the detection of more-complex organic molecules, such as ethanol ( $\text{C}_2\text{H}_5\text{OH}$ ). The frequency of our QC DFB laser falls close to the center of one of the absorption bands of this molecule. Unlike in the ethanol spectrum in the C—H and O—H stretch spectral region ( $\sim 3\text{ }\mu\text{m}$ ), this band has a reasonably well-resolved rovibrational structure. This is explained by the

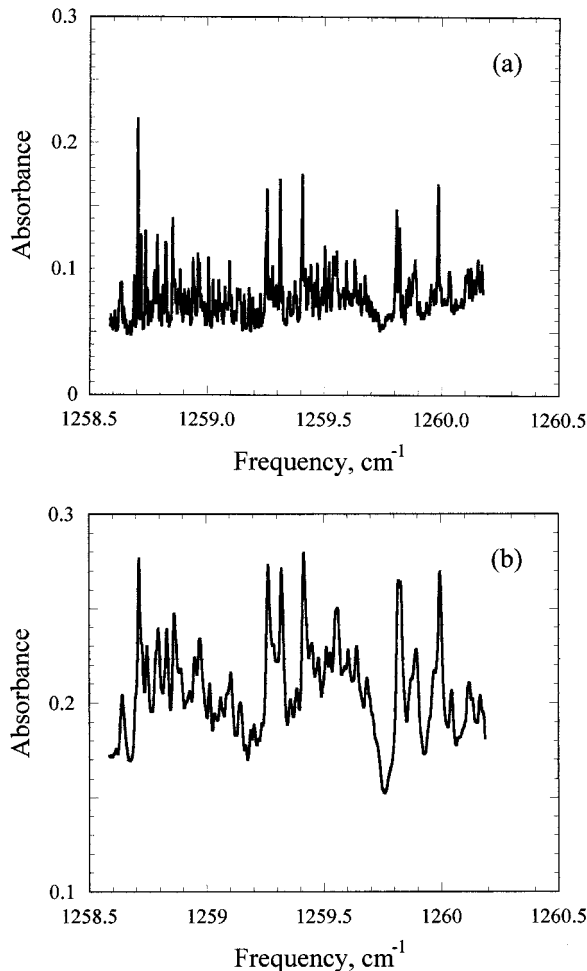


Fig. 5. Ethanol absorption spectra obtained in a 0.43-m-long gas cell: (a) pure ethanol vapor at 1-Torr pressure; (b) same partial pressure of ethanol with room air added to a total pressure of 36.6 Torr.

smaller Doppler width and the much smaller density of vibrational states at  $1200\text{ cm}^{-1}$  than at  $3000\text{ cm}^{-1}$ , where these states already form a vibrational quasi-continuum.<sup>10</sup> Figure 5 shows the ethanol vapor absorption spectra (pure and with ambient air added to a pressure of 36.6 Torr) acquired with our QC DFB laser in a 0.43-m-long gas cell. To increase the ethanol vapor concentration in the laboratory air, we allowed a few drops of ethanol to evaporate near the multipass cell air input as air flowed slowly, but continuously, through the cell, and spectra were acquired 3, 7, 12, and 20 min later at the same 36.6-Torr air pressure in the multipass cell.

The resolved spectral features clearly distinguish the ethanol absorption from that of other species. However, the high density of the pressure-broadened spectral lines makes the technique of individual line fitting with a Voigt profile inapplicable. Therefore we used another approach (suggested by Kosterev) to find the ethanol concentration in air. It is based principally on finding the correlation between previously acquired reference spectra and a spectrum of

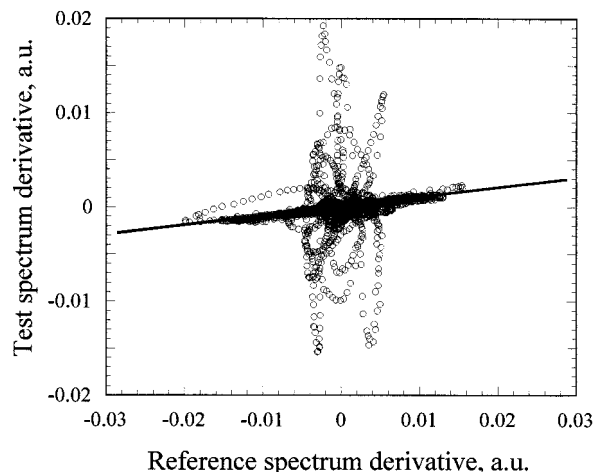


Fig. 6. Value of a test sample spectrum derivative as a function of the reference spectrum derivative. The test sample of room air was taken 7 min after evaporation of a few drops of ethanol near the multipass cell. The fitting line slope yields a value of  $k = 9.82 \times 10^{-2}$ , corresponding to an ethanol concentration of 12.1 ppm.

the sample under investigation (we shall call it a test spectrum) under the same line-broadening conditions (same air pressure and temperature). Various correlation techniques (chemometric methods) have been widely applied to the analysis of low-resolution near-IR spectra of liquid samples and are usually mathematically and computationally complicated (see, for example, Refs. 11 and 12). We propose and demonstrate a relatively simple correlation analysis that to the best of our knowledge was not applied before to high-resolution absorption spectra of gases.

For all data processing procedures described in the following subsections the ethanol absorption spectrum shown in Fig. 5(b) was used as a reference. The reference spectrum comprises 2.87% ethanol vapor by volume in air has a total pressure of 36.6 Torr and a path length of 0.43 m and ranges from 1258.70 to 1260.24  $\text{cm}^{-1}$ . The correlation approach was applied in two modifications: (a) use of one-dimensional linear regression to find a concentration of the ethanol vapor only, and (b) use of multidimensional linear regression (MLR) to find concentrations of all known absorbing species in one fitting procedure.

#### A. One-Dimensional Linear Regression

As a first step of this analysis, we calculated a derivative of each spectral trace by subtracting a 9-data-points-shifted array of data (3650-point total) from the original one. In our experiments, one data-point step equals a  $4.2 \times 10^{-4} \text{ cm}^{-1}$  frequency change. This discrete derivation suppresses the influence of nearly constant background and the slowly changing wings of strong  $\text{H}_2\text{O}$  lines. Subsequently each data-point value from the test spectrum was plotted as a function of the corresponding data-point value from the reference spectrum (Fig. 6). If only ethanol va-

por absorbed the light in the test sample, and no measurement errors were present, all the points of this plot would lie on the straight line  $y = kx$ , where  $k$  is a ratio of ethanol absorbance in two samples. The absorption lines of  $\text{CH}_4$ ,  $\text{N}_2\text{O}$ , and  $\text{H}_2\text{O}$  cause big loops that strongly deviate from this linear law, and measurement errors lead to a scattering of data points. Nevertheless, the large number of points ensures high reliability of the linear fit slope value. Fitting was done in two steps. First, a linear fit was made with all the data points. This step yielded a good estimate of the ethanol concentration, because the strong narrow lines of other species resulted in almost symmetrically scattered points owing to derivation of spectra. Then the points that are distant from the fitting line were considered outliers and excluded from further consideration and the remainder ( $\sim 75\%$  of the initial number) were refitted. In this way the influence of nonethanol absorption lines was minimized. By determining that the slope for samples containing no ethanol fell within a range of  $\pm 1 \times 10^{-3}$  about a zero slope, we could estimate the detection limit as 125 ppb on the basis that a slope of 1 is equal to  $0.0287 \times (0.43\text{m}/100 \text{ m}) \approx 125 \text{ ppm}$  (reference cell ethanol concentration normalized to the ratio of the single-pass and multipass cell optical path lengths).

#### B. Multidimensional Linear Regression

Because the spectra of all the principal absorbing species ( $\text{C}_2\text{H}_5\text{OH}$ ,  $\text{CH}_4$ ,  $\text{N}_2\text{O}$ , and  $\text{H}_2\text{O}$ ) in the frequency range of the laser scan were separately available, a MLR analysis could be applied. Reference spectra of  $\text{CH}_4$ ,  $\text{N}_2\text{O}$ , and  $\text{H}_2\text{O}$  were simulated with HITRAN data. The test spectrum was considered a linear combination of four reference spectra of the absorbing species:

$$y_i = a_0 + \sum_{k=1}^4 a_k x_{ki}, \quad (1)$$

where  $y_i$  is the  $i$ th data point of the test spectrum;  $a_k$  gives the contribution of each absorbing component to the resulting spectrum;  $k = 1, 2, 3, 4$  corresponds to  $\text{C}_2\text{H}_5\text{OH}$ ,  $\text{CH}_4$ ,  $\text{N}_2\text{O}$ , and  $\text{H}_2\text{O}$ , respectively;  $x_{ki}$  is the intensity of the  $k$ th reference spectrum at the frequency of the  $i$ th data point; and  $a_0$  represents an offset and should be close to zero, because derived spectra were used.

We performed a multidimensional linear fit (MLR) to the data set with MathCad software to find a best-fitting four-dimensional hyperplane described by Eq. (1). Offset  $a_0$  was found to be negligibly small for all the data sets. Table 2 shows the results of the fitting procedure applied to test spectra acquired 7 and 12 min after release of ethanol. The concentrations of all the components except for the ethanol remained practically the same within the measurement errors. The ethanol concentrations found from two different approaches to the analysis of data (one-dimensional regression and MLR) are practically the same for sample 2. Some discrepancy for sample 1 is proba-

Table 2. Concentration Values of Trace-Gas Species in Air Samples from Two Different Data Analysis Approaches\*

Species	Measured Concentration			
	Sample 1		Sample 2	
	MLR	One-Dimensional Regression	MLR	One-Dimensional Regression
C <sub>2</sub> H <sub>5</sub> OH	11.60 × 10 <sup>-6</sup>	12.12 × 10 <sup>-6</sup>	1.44 × 10 <sup>-6</sup>	1.41 × 10 <sup>-6</sup>
CH <sub>4</sub>	1.72 × 10 <sup>-6</sup>	–	1.70 × 10 <sup>-6</sup>	–
N <sub>2</sub> O	0.302 × 10 <sup>-6</sup>	–	0.301 × 10 <sup>-6</sup>	–
H <sub>2</sub> O	1.72 × 10 <sup>-3</sup>	–	1.73 × 10 <sup>-3</sup>	–

\*Samples 1 and 2 were taken 7 and 12 min, respectively, after release of ethanol.

bly caused by the influence of nonethanol lines on the one-dimensional linear regression. It should be noted that the relative error for the CH<sub>4</sub>, N<sub>2</sub>O and H<sub>2</sub>O concentrations is greater than that for ethanol because of the smaller number of points involved and also because of small shifts of line positions for the test and simulated reference spectra.

### 5. Conclusions

We have demonstrated what is to our knowledge the first successful application of a single-frequency QC DFB laser to the analysis of trace gases in ambient air. A relatively simple apparatus, consisting of a liquid-nitrogen Dewar with optical access, a laser current driver, and a pulse generator, was used to operate the QC DFB laser. The QC DFB laser-based gas sensor demonstrated detection sensitivity to the air components of 2.5 ppb for CH<sub>4</sub>, 1.0 ppb for N<sub>2</sub>O, and 60 ppb for H<sub>2</sub>O (~60-s data acquisition time). The feasibility of spectroscopic isotopic composition measurements of atmospheric H<sub>2</sub>O and CH<sub>4</sub> was demonstrated, although making them useful will require improvements. A new technique for data analysis of dense absorption spectra was proposed and implemented. This approach resulted in a 125-ppb detection limit for ethanol.

Financial support of the research performed by the authors at Rice University was provided by the National Aeronautics and Space Administration, the Institute for Space Systems Operations, the Texas Advanced Technology Program, the National Science Foundation, and the Welch Foundation. The Bell Laboratories team received partial support from the Defense Advanced Research Projects Agency/U.S. Army Research Office under grant DAA G 55-98-C-0050.

### References

1. F. Capasso, C. Gmachl, D. L. Sivco, and A. Y. Cho, "Quantum cascade lasers," *Phys. World* **12**, 27–33 (1999); F. Capasso, C. Gmachl, A. Tredicucci, A. L. Hutchinson, D. L. Sivco, and A. Y. Cho, "High performance quantum cascade lasers," *Opt. Photon. News* **10**(10), 32–37 (1999).

2. A. A. Kosterev, R. F. Curl, F. K. Tittel, C. Gmachl, F. Capasso, D. L. Sivco, J. N. Baillargeon, A. L. Hutchinson, and A. Y. Cho, "Methane concentration and isotopic composition measurements with a mid-infrared quantum cascade laser," *Opt. Lett.* **24**, 1762–1764 (1999).
3. B. A. Paldus, T. G. Spence, R. N. Zare, J. Oomens, F. J. M. Harren, D. H. Parker, C. Gmachl, F. Capasso, D. L. Sivco, J. N. Baillargeon, A. L. Hutchinson, and A. Y. Cho, "Photoacoustic spectroscopy using quantum-cascade lasers," *Opt. Lett.* **24**, 178–180 (1999).
4. S. W. Sharpe, J. F. Kelly, J. S. Hartman, C. Gmachl, F. Capasso, D. L. Sivco, J. N. Baillargeon, and A. Y. Cho, "High-resolution (Doppler-limited) spectroscopy using quantum-cascade distributed-feedback lasers," *Opt. Lett.* **23**, 1396–1398 (1998).
5. K. Namjou, S. Cai, E. A. Whittaker, J. Faist, C. Gmachl, F. Capasso, D. L. Sivco, and A. Y. Cho, "Sensitive absorption spectroscopy with a room-temperature distributed-feedback quantum-cascade laser," *Opt. Lett.* **23**, 219–221 (1997).
6. A. Fried, S. Sewell, B. Henry, B. P. Wert, T. Gilpin, and J. R. Drummond, "Tunable diode laser absorption spectrometer for ground-based measurements of formaldehyde," *J. Geophys. Res.* **102**, 6253–6266 (1997).
7. P. Bergamaschi, M. Schupp, and G. W. Harris, "High-precision direct measurements of <sup>13</sup>CH<sub>4</sub>/<sup>12</sup>CH<sub>4</sub> and <sup>12</sup>CH<sub>3</sub>D/<sup>12</sup>CH<sub>4</sub> ratios in atmospheric methane sources by means of a long-path tunable diode laser absorption spectrometer," *Appl. Opt.* **33**, 7704–7716 (1994).
8. P. Fritz and J. Ch. Fontes, eds., *Handbook of Environmental Isotope Geochemistry* (Elsevier, New York, 1980), Vol. 1, pp. 1–19.
9. International Atomic Energy Agency and World Meteorological Organization, *Global Network for Isotopes in Precipitation. The GNIP Database* release 3, October 1999, <http://www.iaea.org/programs/ri/gnip/gnipmain.htm>.
10. A. A. Stuchebrukhov; S. I. Ionov, and V. S. Letokhov, "IR spectra of highly vibrationally excited large polyatomic molecules and intramolecular relaxation," *J. Phys. Chem.* **93**, 5357–5365 (1989).
11. M. Kubista, J. Nygren, A. Elbergali, and R. Sjöback, "Making reference samples redundant," *Crit. Rev. Anal. Chem.* **29**, 1–28 (1999).
12. M. J. McShane, G. L. Coté, and C. H. Spiegelman, "Assessment of partial least-squares calibration and wavelength selection for complex near-infrared spectra," *Appl. Spectrosc.* **52**, 878–884 (1998).